Research Article

GAZİ
JOURNAL OF ENGINEERING SCIENCES

Design and Preliminary Validation of a UAV-Based System for Remote Animal Anesthesia

Nihat Çabuk[*a]

Submitted: 07.11.2024 **Revised :** 29.05.2025 **Accepted:** 09.07.2025 **doi:**10.30855/gmbd.070525A05

[a,*] Aksaray University, Vocational School of Technical Sciences, Dept. of Electricity and Energy 68200 - Aksaray, Türkiye, Orcid: 0000-0002-3668-7591
Corresponding author: nihatcabuk@aksaray.edu.tr

Keywords: Animal anesthesia, UAV, design, control, simulation

ABSTRACT

In this study, a quadrotor unmanned aerial vehicle (UAV)-based system is proposed to perform remote anesthesia on animals located in areas with limited accessibility. The system integrates a robotic manipulator and a needle-launching mechanism into the UAV platform. The developed model incorporates UAV dynamics, forward and inverse kinematics of the manipulator, and a simplified linear motion assumption for the needle. Simulation studies were conducted for two scenarios: a stationary and a moving target. In both cases, manipulator joint angles were computed in real time based on UAV flight data. Results show successful alignment of the injector mechanism with the target, and they highlight the influence of the reaction force during needle launching on UAV stability. In the experimental phase, a Pixhawk flight controller and Lua scripting were used to calculate joint angles using live telemetry data. While real needle firing was not performed due to safety concerns, the manipulator's ability to track a fixed target was validated. This proof-of-concept study provides a foundation for future systems that can incorporate autonomous vision-based tracking and live in-flight deployment, contributing to more efficient and humane wildlife management practices.

Abbreviations and Notations

UAV	Unmanned Aerial Vehicle
FMU	Flight Management Unit
FCU	Flight Control Unit
GPS	Global Positioning System
RC	Radio control
ESC	Electronic speed controller
CoM	Centre of Mass
DH	Denavit-Hartenberg
RPM	Rotate per Minute
F_i	i.th motor thrust force
M_r	Roll moment
M_p	Pitch moment
M_y	Yaw moment
${}^{e}\boldsymbol{P}_{v,i}$	Position vector of the UAV for i.th step on Earth Frame
${}^{e}\boldsymbol{P}_{t,i}$	Position vector of the target for i.th step on Earth Frame
q_1	First joint angle of the manipulator
q_2	Second joint angle of the manipulator
φ, θ and ψ	Euler angels
Thr	Throttle
k_f, k_m	thrust and reverse moment coefficient
Ω_i	Angular velocity of i.th rotor of UAV
${}^{e}_{b}\boldsymbol{R}$	Rotation matrix of Earth to Body Frame of UAV
${}^{i}_{i+1}\boldsymbol{T}$	Homogeneous transformation matrix i.th to (i+1).th frame

To cite this article: N. Çabuk, "Design and Preliminary Validation of a UAV-Based System for Remote Animal Anesthesia", *Gazi Journal of Engineering Sciences,* vol.11, no.2, pp. 188-205, 2025. doi:10.30855/gmbd.070525A05

1. Introduction

Unmanned aerial vehicles (UAVs) are highly innovative vehicles that are remotely controlled and come in a wide range of take-off weights. They are classified into two main categories: fixed-wing and rotary-wing, depending on the number of rotors they possess [1,2]. While each category has its own strengths and weaknesses, the choice of UAV depends on their specific application areas and advantages. These vehicles can be designed in various physical structures to enhance their effectiveness [3–7]. The utilization of UAVs, both in civilian and military contexts, continues to increase. Moreover, the integration of different devices into UAVs expands their range of applications [8–15]. Initially, UAVs were primarily used for imaging by incorporating cameras [16–19]. Over time, they are employed for sample collection [20,21] and object transport [22–24] by attaching various grippers [25–27]. Similarly, their usage in agricultural practices, such as seed scattering and spraying, becomes more widespread [28–32]. Furthermore, with the installation of weapon systems on these vehicles, their military applications have also emerged [33].

Figure 1. Example of a gun for anesthesia of animals

In fact, UAVs can be assigned tasks in areas that may pose challenges or risks to humans. One such area involves UAV systems that undertake various tasks related to animals [34–37]. Anesthesia [38–40] of uncontrollable or temporarily incapacitated animals represents another challenging and hazardous task. For instance, capturing wild animals in nature, handling stray animals, or returning escaped farm animals to their designated areas often necessitates the use of a needle-throwing gun for anesthesia, as depicted in Figure 1 [41].

The current task is predominantly performed using land vehicles and personnel on foot, posing significant challenges for officials involved. However, in situations where access is limited by both foot and vehicle, these tasks often yield unsuccessful outcomes. A literature review revealed limited studies on the proposed system within the scope of this research. To enhance the success rate of this task, the present study proposes the utilization of a UAV system.

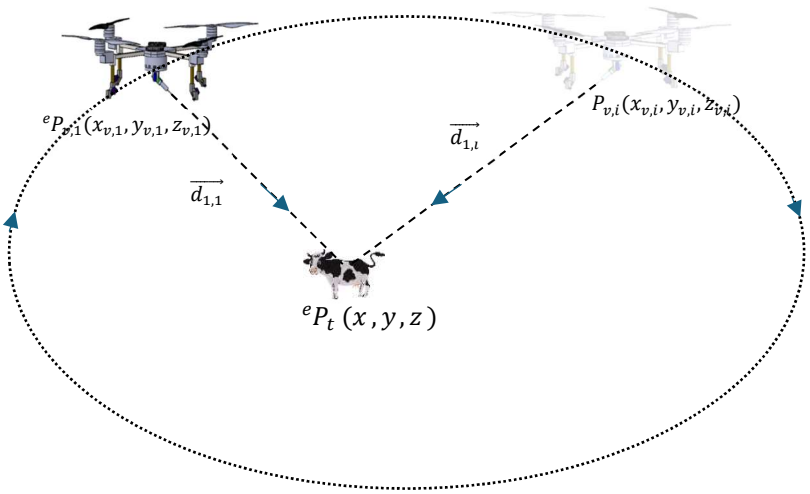

Figure 2. Working principle of the system

The aim is to facilitate the capture of target animals through remote anesthesia, allowing officials to perform the necessary procedures. The proposed system comprises three key components: a quadrotor UAV system, a manipulator, a needle throwing mechanism. Figure 2 provides a visual representation of the proposed system in action.
This study on the proposed system comprises four main sections: "Description of Proposed System," "Simulation Study and Results," "Experimental Setup", and "Discussion and Conclusion."

In "Description of Proposed System" section, the physical structure of the entire proposed system is outlined, and a mathematical model of the system is derived. The components of the system include the quadrotor UAV, a manipulator, and needle throwing mechanism. The manipulator incorporates a rotary joint driven by a servo motor. The angular positions of these joints are determined based on the target animal's position, as well as the linear and angular positions of the UAV. In this study, the effects of factors like aerodynamics and gravity on the motion of the thrown needle are not considered. Instead, the focus is on the reaction force resulting from the throwing action. Consequently, a mathematical model is developed, assuming linear motion for the thrown needle.

Simulation Study and Results section presents the simulation study conduct on the proposed system, which involved running simulations in two different scenarios. The objective is to demonstrate the validity and effectiveness of the system. Details of the simulations, along with the obtained results, are provided.
In, Experimental Setup section, the production and assembly of the proposed system is presented. The working principle of the real system is mentioned. The final section, Discussion and Conclusion, offers an evaluation and discussion of the study's findings. Conclusions are drawn based on the outcomes of the simulations and the performance of the proposed system. Additionally, potential limitations and suggestions for future improvements may be discussed.

2. Description of Proposed System

The entire system consists of four subsystems: the quadrotor UAV, a manipulator, needle throwing mechanism, and camera, as shown in Fig. 3. The manipulator incorporates a rotary joint driven by a servo motors. The angular positions of these joints are determined based on the position of the target animal, as well as the linear and angular positions of the UAV. These joint angles are calculated using inverse kinematic calculations. It is important to note that when an arrow is thrown, it is influenced by aerodynamics and gravity throughout its trajectory [42,43]. A more realistic model would require solving the projectile motion equations under gravity and aerodynamic drag:

$$m\frac{d\vec{v}}{dt} = m\vec{g} - \frac{1}{2}C_d\rho A\|\vec{v}\|\vec{v} \tag{1}$$

where C_d is the drag coefficient, ρ is the air density, and A is the cross-sectional area of the needle. Implementing this level of modeling is planned for future work as part of dynamic system refinement. In this study, the trajectory of the launched needle is modeled as a linear path. This simplification assumes that external forces such as gravity and aerodynamic drag are negligible, which may not reflect the actual motion of a needle in real-world scenarios, particularly when launched from a moving UAV at a non-zero altitude. The linear model is defined by:

$$\vec{r}\,(t) = \vec{r}_0 + \vec{v}_0 t \tag{2}$$

where $\vec{r}_0$ is the initial position of the needle, and v ⃗_0 is its initial velocity vector. Although this model simplifies the trajectory calculation, it serves as a first-order approximation suitable for evaluating the basic alignment and response of the manipulator system. Thus, assuming that the thrown needle follows a linear trajectory, a mathematical model of the entire system has been developed.

ISSN: 2149-9373

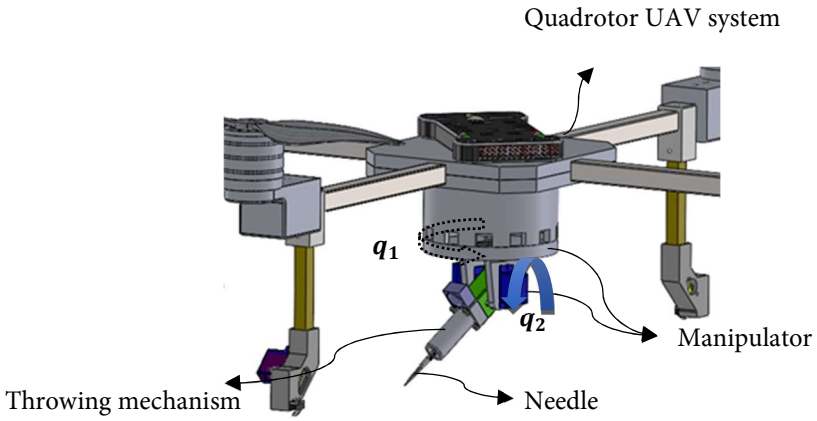

Figure 3. Demonstration of the whole system

2.1. System model

The solid model of the proposed system is depicted in Fig. 4. In the figure, φ, θ and, ψ represent the Euler angles, while q_1 and q_2 denote the angular variables of the manipulator's joint. The variable d_1represents the distance between the needle throwing mechanism and the target animal. The kinematics of a system with angular and/or linear joints rely on both the joint variables and mechanical constants. As shown in Figure 4, when defining the position of the target animal in relation to the UAV's position, a mathematical expression needs to be derived to describe the relationship between these two positions using assigned coordinate axes. To achieve this, two axis sets, $\{M_1\}$ and $\{M_2\}$, must be designated at positions where there are variables between the two positions. The rotation (orientation) involving roll, pitch, and yaw between the Earth-fixed axis set and the body-fixed axis set of the UAV is represented by Euler angles. The matrix representing this rotation is presented in (3) and (4). The linear position difference between these axes is expressed by latitude, longitude, and altitude, as given in (5). The instantaneous values of all six variables are obtained from the flight control unit.

$$R_{yaw} = \begin{pmatrix} c\psi & s\psi & 0 \\ -s\psi & c\psi & 0 \\ 0 & 0 & 1 \end{pmatrix}, R_{pitch} = \begin{pmatrix} c\theta & 0 & -s\theta \\ 0 & 1 & 0 \\ s\theta & 0 & c\theta \end{pmatrix}, R_{roll} = \begin{pmatrix} 1 & 0 & 0 \\ 0 & c\varphi & s\varphi \\ 0 & -s\varphi & c\varphi \end{pmatrix} \quad (3)$$

Considering that s• and c• represent sin• and cos•, respectively, the rotation matrix representing the rotation between the Earth-fixed axis set and the body-fixed axis set can be expressed as follows:

$${}^{e}_{b}R(\varpi) = \begin{pmatrix} c\theta c\psi & c\theta s\psi & -s\theta \\ s\varphi s\theta c\psi - c\varphi s\psi & s\varphi s\theta s\psi + c\varphi c\psi & s\varphi c\theta \\ c\varphi s\theta c\psi + s\varphi s\psi & c\varphi s\theta s\psi - s\varphi c\psi & c\varphi c\theta \end{pmatrix} \quad (4)$$

$\varpi = [\varphi, \theta, \psi\,]$ represents the attitudes of the quadrotor.

$${}^{e}P_{borg} = [{}^{e}P_{v,x}\ {}^{e}P_{v,y}\ {}^{e}P_{v,z}]^{T} \quad (5)$$

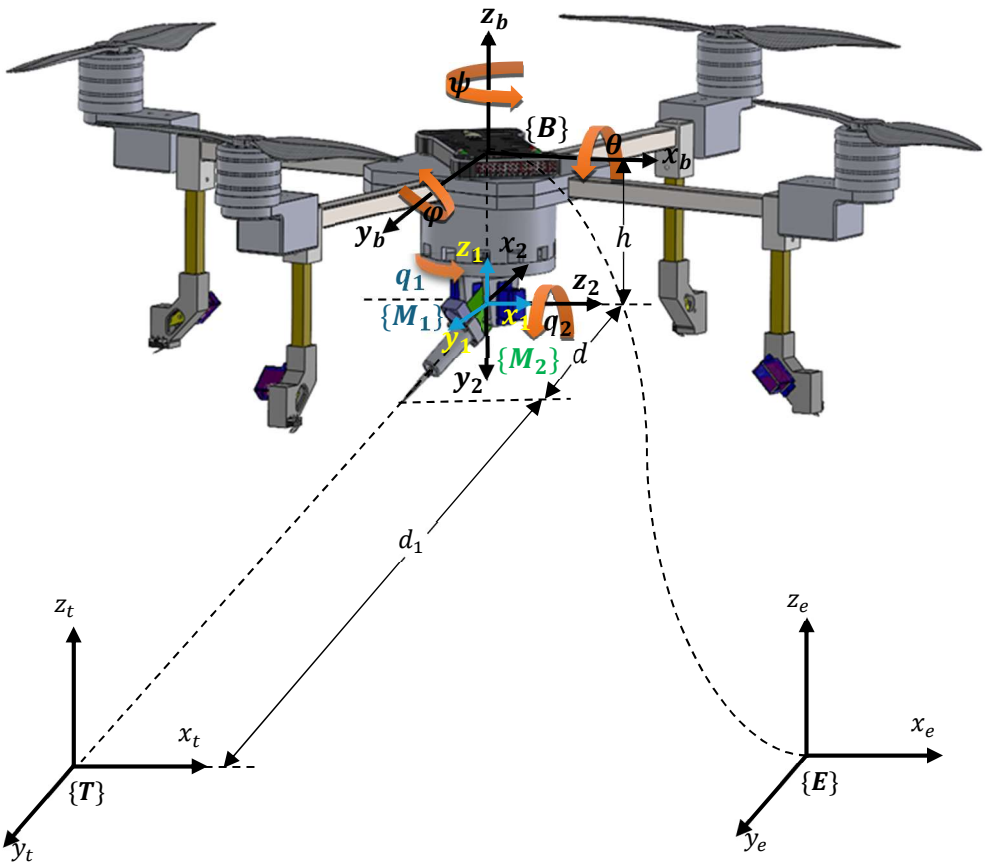

Figure 4. The solid model and identification of the proposed system

To obtain the homogeneous transformation matrix, incorporating both the orientation matrix and the position vector, it can be done using (6) and (7).

$$ {}^{e}_{b}T = \begin{bmatrix} {}^{e}_{b}R & {}^{e}P_{borg} \\ 0\,0\,0 & 1 \end{bmatrix} \tag{6} $$

$$ {}^{e}_{b}T = \begin{bmatrix} c\theta c\psi & c\theta s\psi & -s\theta & {}^{e}P_{v,x} \\ s\varphi s\theta c\psi - c\varphi s\psi & s\varphi s\theta s\psi + c\varphi c\psi & s\varphi c\theta & {}^{e}P_{v,y} \\ c\varphi s\theta c\psi + s\varphi s\psi & c\varphi s\theta s\psi - s\varphi c\psi & c\varphi c\theta & {}^{e}P_{v,z} \\ 0 & 0 & 0 & 1 \end{bmatrix} \tag{7} $$

The transformation matrix from the body frame to the target frame, considering the joint variables of the manipulator and the mechanical properties of the limbs, can be obtained. The transformation matrices between the three-dimensional axes assigned to the manipulator joints are determined, and a homogeneous transformation matrix is derived from the body frame to the target frame.

2.2. Forward kinematics

In (8), ${}^{b}_{t}T$ represents the homogeneous transformation matrix that contains the position and orientation of the target with respect to the UAV body frame. The joint angles of the manipulator, denoted as $Q = [q_1, q_2, d_1]$, are used to define the transformation matrix.

$$ {}^{b}_{t}T(Q) = {}^{b}_{M_1}T(q_1) * {}^{M_1}_{M_2}T(q_2) * {}^{M_2}_{t}T(d_1) \tag{8} $$

The Denavit-Hartenberg (DH) model is a well-known and widely used approach for describing the kinematics of robotic manipulators. By applying the DH model, the kinematics of the manipulator can be effectively represented. The DH model relies on assigning coordinate frames and defining transformation matrices between consecutive frames along the manipulator's links. Each link is represented by a homogeneous transformation matrix, which relates the frame attached to the link with the frame fixed to the link. The DH parameters, including link lengths, link twists, link offsets, and joint angles, are used to determine these transformation matrices. By sequentially multiplying the transformation matrices based on the DH parameters, the forward kinematics of the manipulator can be computed, providing the end-effector's position and orientation. Although physically not a joint, the translation variable d_1 can accommodate additional degrees of freedom in the manipulator as a member of the DH parameters. Thus, the transformation matrices between successive joints are obtained as follows.

$$ d_1 = \sqrt{\left(({}^{e}P_{v,x} - {}^{e}P_{t,x})^2 + ({}^{e}P_{v,y} - {}^{e}P_{t,y})^2 + ({}^{e}P_{v,z} - {}^{e}P_{t,z})^2\right)} \tag{9} $$

$$ {}^{b}_{M_1}T = \begin{bmatrix} cq_1 & -sq_1 & 0 & 0 \\ sq_1 & cq_1 & 0 & 0 \\ 0 & 0 & 1 & -h \\ 0 & 0 & 0 & 1 \end{bmatrix}, {}^{M_1}_{M_2}T = \begin{bmatrix} cq_2 & -sq_2 & 0 & 0 \\ 0 & 0 & -1 & 0 \\ sq_2 & cq_2 & 1 & 0 \\ 0 & 0 & 0 & 1 \end{bmatrix}, {}^{M_2}_{t}T = \begin{bmatrix} 1 & 0 & 0 & 0 \\ 0 & 0 & 1 & -(d+d_1) \\ 0 & -1 & 0 & 0 \\ 0 & 0 & 0 & 1 \end{bmatrix} \tag{10} $$

$$ {}^{b}_{t}T = \begin{bmatrix} cq_1cq_2 & -sq_1 & -cq_1sq_2 & cq_1sq_2(d+d_1) \\ cq_2sq_1 & cq_1 & -sq_1sq_2 & sq_1sq_2(d+d_1) \\ sq_2 & 0 & cq_2 & -h - cq_2(d+d_1) \\ 0 & 0 & 0 & 1 \end{bmatrix} \tag{11} $$

$$ {}^{e}_{t}T = \begin{bmatrix} r_{11} & r_{12} & r_{13} & {}^{e}P_{t,x} \\ r_{21} & r_{22} & r_{23} & {}^{e}P_{t,y} \\ r_{31} & r_{32} & r_{33} & {}^{e}P_{t,z} \\ 0 & 0 & 0 & 1 \end{bmatrix} = {}^{e}_{b}T(\varpi) * {}^{b}_{t}T(Q) \tag{12} $$

In the equations, ${}^{e}P_{t,n}$ and ${}^{e}P_{v,n}$ are the position of the target and the UAV according to the earth coordinate system, respectively, where n takes values x, y, or z. And ${}^{e}P_{v,n}$ data is taken instantly from the flight controller unit (FCU).

2.3. Inverse kinematics

In calculating the manipulator joint angles, inverse kinematic operations are performed using the position data of the UAV and the target. The inverse kinematics process involves determining the joint angles of the manipulator based on the desired position and orientation of the end-effector or target. By applying inverse kinematics, the joint angles can be computed to achieve the desired positioning of the manipulator [44,45].
The following equation is obtained to calculate of inverse equation for q_1, q_2 angels.

$$ [{}^{e}_{b}T * {}^{b}_{M_1}T]' * {}^{e}_{t}T = {}^{M_1}_{M_2}T * {}^{M_2}_{t}T \tag{13} $$

By equalizing the 2nd row and 4th column elements of both matrices obtained, the inverse kinematic equation is obtained for q_1. For the sake of simplicity of the inverse equations, Ƙ and ϐ given in equation 15 are,

$$ \begin{aligned} Ƙ &= {}^{e}P_{t,y}{*}c\varphi{*}c\psi + {}^{e}P_{t,y}{*}s\theta{*}s\varphi{*}s\psi - {}^{e}P_{t,z}{*}c\psi{*}s\varphi - {}^{e}P_{t,z}{*}c\varphi{*}s\theta{*}s\psi \\ ϐ &= {}^{e}P_{t,y}{*}\ c\varphi{*}s\psi - {}^{e}P_{t,y}{*}\ c\psi\ {*}s\theta{*}s\varphi + {}^{e}P_{t,z}{*}s\varphi{*}s\psi - {}^{e}P_{t,z}{*}c\varphi{*}s\psi{*}s\theta \end{aligned} \tag{14} $$

$$q_1 = \text{atan2}(\beta, \text{Ķ}) + \text{acos}\left(-{}^{e}P_{t,x} * c\theta / \sqrt{(\text{Ķ}^2 + \beta^2)}\right) \quad (15)$$

Since angle q_1 is known, similarly, the 1st row 4th column elements of both matrices obtained are equalized to each other to obtain an inverse kinematic equation for q_2.

$$q_2 = \text{asin}(({}^{e}P_{t,x} * (cq_1 * c\theta * c\psi + sq_1 * c\theta * s\psi - {}^{e}P_{t,y} * (cq_1 * c\varphi * s\psi - sq_1 * c\varphi * c\psi * s\theta * s\varphi) - ({}^{e}P_{t,z} - h) * (\quad (16)$$
$$cq_1 * (s\varphi * s\psi + c\varphi * c\psi * s\theta) - sq_1 * (c\psi * s\varphi - c\varphi * s\theta * s\psi))) / (d + d_1))$$

In the equations, the Euler angles and the position of the UAV are taken instantly from the FCU.

3. Dynamics of UAV with Manipulator

The forces and moments in the system are primarily generated by the thrust forces of the propellers, which are proportional to the square of the rotational speeds of the UAV's rotors. The effect of the servo motors in the manipulator joints is considered negligible as they have little impact on these forces and moments. The thrust produced by each propeller (F_i) and the reverse moment effect caused by each rotor-propeller pair ($M_{y,i}$) can be calculated using the thrust coefficient (k_f) and the reverse moment coefficient (k_m) as follows:
Thrust of each propeller: $F_i = k_f \Omega_i{}^2$
Reverse moment effect of each rotor-propeller pair: $M_{y,i} = k_m \Omega_i{}^2$. Where T_i represents the thrust produced by the i-th propeller. $M_{y,i}$ represents the reverse moment (yaw effect) caused by the i-th rotor-propeller pair. Ω_i represents the rotational speed of the i-th rotor.

Considering a quad-rotor UAV, as is relevant for this study, the total thrust (T_t) and total reverse moment (M_y) can be calculated by summing the contributions from each propeller or rotor-propeller pair, respectively:

$$T_t = \sum_{i=1}^{4} k_f \Omega_i{}^2 \ (\text{for } i = 1 \text{ to } 4)$$
$$M_y = \sum_{i=1}^{4} (-1)^i \, k_m \Omega_i{}^2 \ (\text{for } i = 1 \text{ to } 4) \quad (17)$$

Differences in the rotational speeds of each of the four rotors can lead to roll (M_r) and pitch (M_p) moments. These moments arise due to asymmetrical thrust forces generated by the rotors. When the rotational speeds of the rotors are not identical, the resulting imbalances in thrust cause the UAV to experience roll and pitch motions. Additionally, the reaction force (F_r) exerted by the throwing mechanism during the needle-throwing process can have an impact on the total thrust forces and the roll and pitch moments of the UAV. The specific effect of the throwing mechanism's reaction force on the UAV's dynamics depends on the joint angles of the manipulator. It's important to consider these factors when analyzing and controlling the quad-rotor UAV system, as they contribute to the overall stability and maneuverability of the UAV during operation.

$$\begin{bmatrix} F_t \\ M_r \\ M_p \\ M_y \end{bmatrix} = [\text{A}] * \begin{bmatrix} \Omega_1{}^2 \\ \Omega_2{}^2 \\ \Omega_3{}^2 \\ \Omega_4{}^2 \end{bmatrix} + \begin{bmatrix} F_r \, sq_2 \\ F_r \, cq_2 hc(\psi - q_1) \\ F_r \, cq_2 hs(\psi - q_1) \\ 0 \end{bmatrix} \quad (18)$$

The matrix A is associated with the physical structure of the UAV. To simplify the notation, the expression $\Gamma = l * \text{s}(\frac{\pi}{2})$ has been introduced as an abbreviation.

In this abbreviation, l represents the shortest distance between the geometric center of the UAV and the rotation axis of

a rotor, while s is a scaling factor. By using this abbreviation, the matrix A in (19) can be written more simply. However, without the specific equation or further details of the matrix A and its purpose within the context of the UAV's physical structure, it is challenging to provide a more specific explanation or application.

A diagram of the control of the whole system is given in Figure 5. In the control diagram, U_d represents the desired moments and force value vector for the UAV, given by $U_d = [F_t\ M_r\ M_p\ M_y]^T$.

$$\mathrm{A} = \begin{bmatrix} k_f & k_f & k_f & k_f \\ -\Gamma & \Gamma & \Gamma & -\Gamma \\ \Gamma & -\Gamma & \Gamma & -\Gamma \\ -k_m & -k_m & k_m & k_m \end{bmatrix} \tag{19}$$

This vector includes the desired values for the total forces, roll moment, pitch moment, and yaw moment of the UAV. The net force acting on the UAV consists of four components, the thrust that is produced by the propellers, gravitational forces, disturbing forces and reaction force of throwing mechanism. The translational equations of the whole system are obtained from equation 20. The drag force caused by the UAV body is not considered. In (17), $\omega_b = [p\ q\ r]^T$ and $V_b = \begin{bmatrix} V_x\ V_y\ V_z\ \end{bmatrix}^T$ are angular and

$$\begin{aligned} F_b &= F_t - ({}^e_bR\ \times\ mg) \\ \dot{V}_b &= \left({}^{F_b}/_{m}\right) - (\omega_b \times V_b) \end{aligned} \tag{20}$$

translation velocity vectors, respectively. Similarly, moments acting on the vehicle due to the thrust and reaction force of throwing mechanism are roll and pitch moments. In addition to the moments, there are gyroscopic moments which may not be considered. The angular equations of the whole system are obtained as in (21).

$$\begin{aligned} M_b &= \begin{bmatrix} \sum_{i=1}^{4}(-(-1)^i \times (I_{zz} \times p \times \Omega_i)) \\ \sum_{i=1}^{4}((-1)^i \times (I_{zz} \times q \times \Omega_i)) \\ \sum_{i=1}^{4}(-(-1)^i \times (I_{zz} \times \dot{\Omega}_i)) \end{bmatrix} + \begin{bmatrix} M_r \\ M_p \\ M_y \end{bmatrix} \\ \dot{\omega}_b &= \left({}^{M_b}/_{I}\right) - \left({}^{(\omega_b \times I\omega_b)}/_{I}\right) \end{aligned} \tag{21}$$

4. Simulation Study and Results

Simulations were conducted to validate the entire system, utilizing the obtained mathematical model. Two distinct scenarios were defined for the simulations. The first scenario involved a fixed-position target, while the second scenario involved a target that was in motion across all three dimensions. In both simulations, the UAV autonomously flew along a predetermined trajectory. As the UAV approached a specific distance along the trajectory, the throwing mechanism become active. Additionally, during autonomous flight, the manipulator joint angles, which are responsible for positioning the needle throwing mechanism, were instantaneously determined to align the mechanism with the target. The simulation utilized the physical parameters of the UAV, as outlined in Table 1.

ISSN: 2149-9373

Table 1. Physical parameters of whole UAV system

Parameters||Describing	Symbol	Value	Unit
Thrust coefficient	k_f	0.9412e-04	N/(rad/sec)^2
Reverse moment coefficient	k_m	3.0522e-06	Nm/(rad/sec)^2
Total max thrust	F_t	72	N
Rotor RPM value per volt	KV	720	Rpm/V
Total mass of whole UAV system	m	1690	g
Throwing mechanism reaction force	F_r	10	N
Length of the arm to which the motor is attached	l	360	mm
Length of second limb of the manipulator	d	100	mm
Distance of CoM of UAV to Manipulator second joint	h	100	mm

The block diagram of the whole system related to the simulation is given in Figure 5.

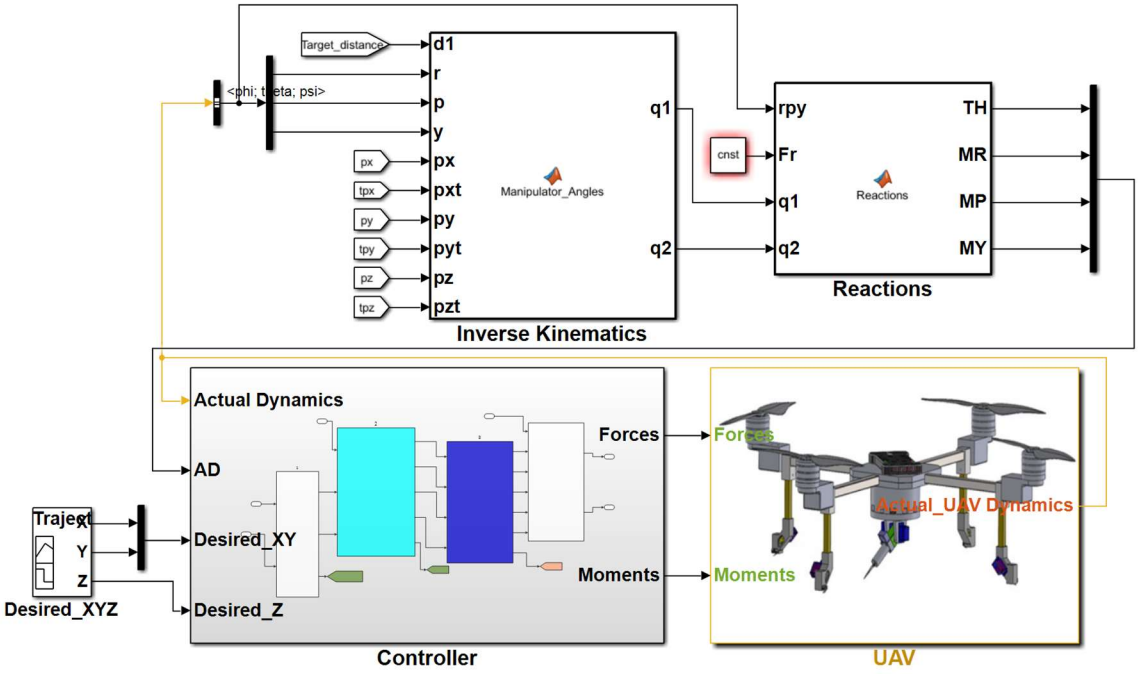

Figure 5. Controller structure of the proposed system for simulation

In the simulation phase, the launch mechanism activation is governed by a dual-condition logic implemented through Lua scripting and MATLAB-based control simulation. The conditions are as follows:

$$D = \sqrt{(x_v - x_t)^2 + (y_v - y_t)^2 + (z_v - z_t)^2} < D_{threshol} \quad (22)$$

Distance conditions:

where $D_{threshold}$ determined as approximately 20 m, although it may vary depending on the characteristics of the shooting mechanism to be used. This ensures that the UAV is within an effective range of the target.
Alignment condition:

Let $\vec{l}$ be the direction vector of the manipulator's end-effector and $\vec{r}$ the vector from the end-effector to the target. As seen in fig 4, the angle q_2 between these two vectors satisfies:

$$q_2 = \arccos\left(\frac{\vec{l}.\vec{r}}{\|\vec{l}\|.\|\vec{r}\|}\right) < q_{2max} \tag{23}$$

where q_{max}~3°, then the alignment is considered acceptable. Once both conditions are met, the launch mechanism is triggered. This logical framework is embedded in the simulation to replicate a real-world decision-making mechanism under simplified assumptions.

Stationary state of the target

In the stationary target scenario, the target remains fixed at ${}^{e}P_t(40, 35, 0)$ relative to the reference zero position. As the UAV autonomously follows a predetermined trajectory, the manipulator joint angles are instantaneously determined based on the positional difference between the UAV and the target.

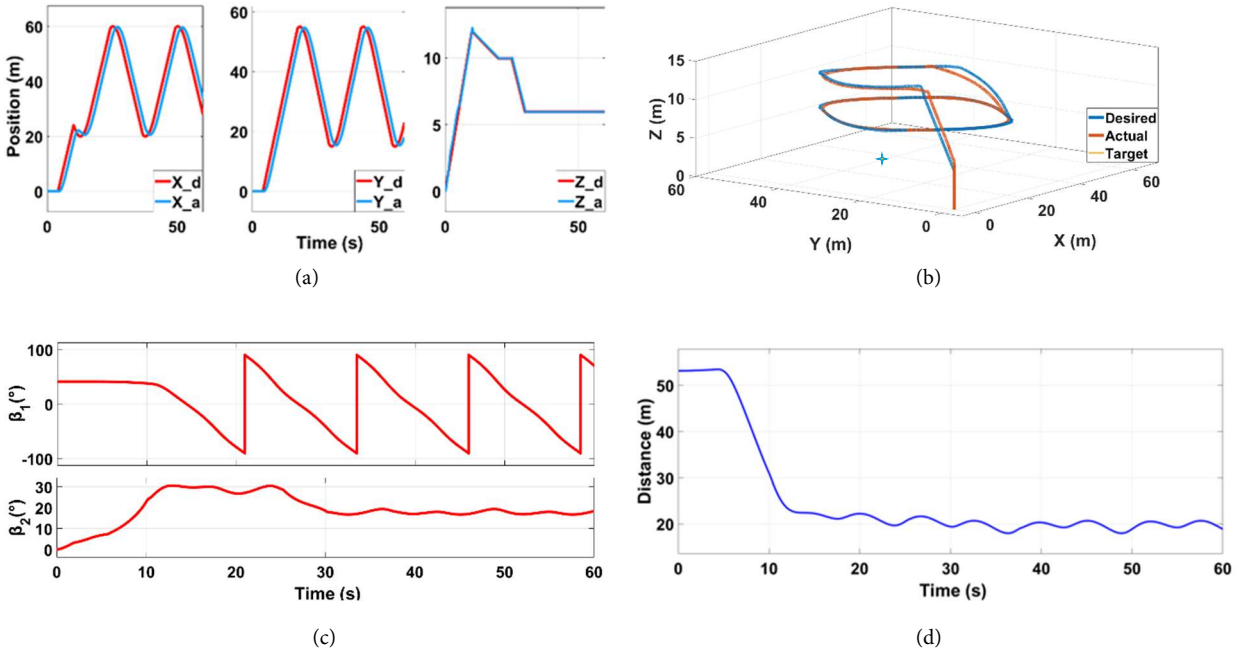

Figure 6. Regarding the condition of the target being fixed; Trajectory tracking graphic (a) and (b), change in manipulator joint angles (c), change in distance between UAV and target (d)

Figure 6 provides visual representations of the scenario: The reference trajectory for each of the three axes separately (a). The reference trajectory and the trajectory followed by the UAV in three dimensions (b). The values of the manipulator joint angles (c). The linear distance between the UAV and the target, which changes over the course of the flight time (d).

In Fig. 7, two sets of information are presented to provide insight into the flight dynamics and the effect of the throw reaction force: The subplot, Fig. 7a, illustrates the changes in the roll, pitch, and yaw angles of the UAV throughout the flight. The plot showcases how these angles evolve over time, capturing the UAV's orientation and rotational movements along each axis. The subplot, Fig. 7b, highlights the impact of the throw reaction force on the moments (roll, pitch, and yaw) and the thrust force of the UAV. It demonstrates how the throw reaction force influences the UAV's stability and control by exerting moments and affecting the thrust force.

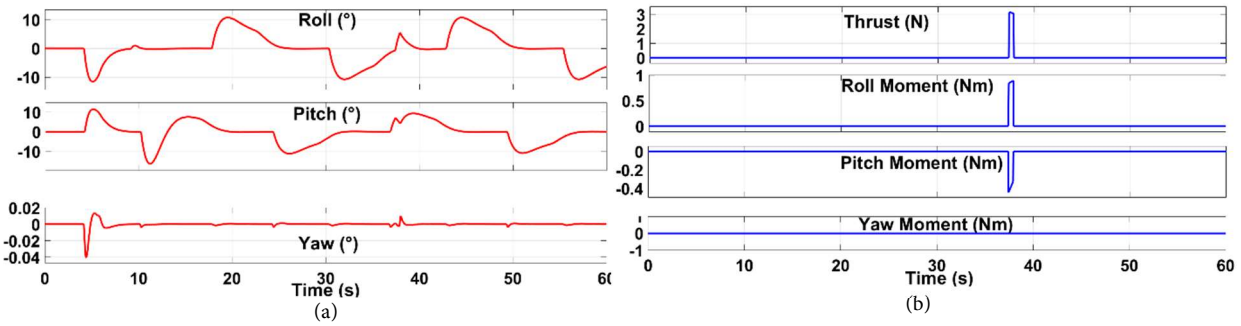

(a) (b)

Figure 7. Case of the fixed target; Euler angles change graph (a), the effect of throw reaction force on roll, pitch and yaw moments, and thrust force (b)

Moving state of the target

In the moving target scenario, it is realistic for the target to change its position by making different movements. To simulate this situation, similar to the first simulation, the UAV autonomously follows the same orbit trajectory. Additionally, a path is determined to represent the movement of the target in three dimensions.

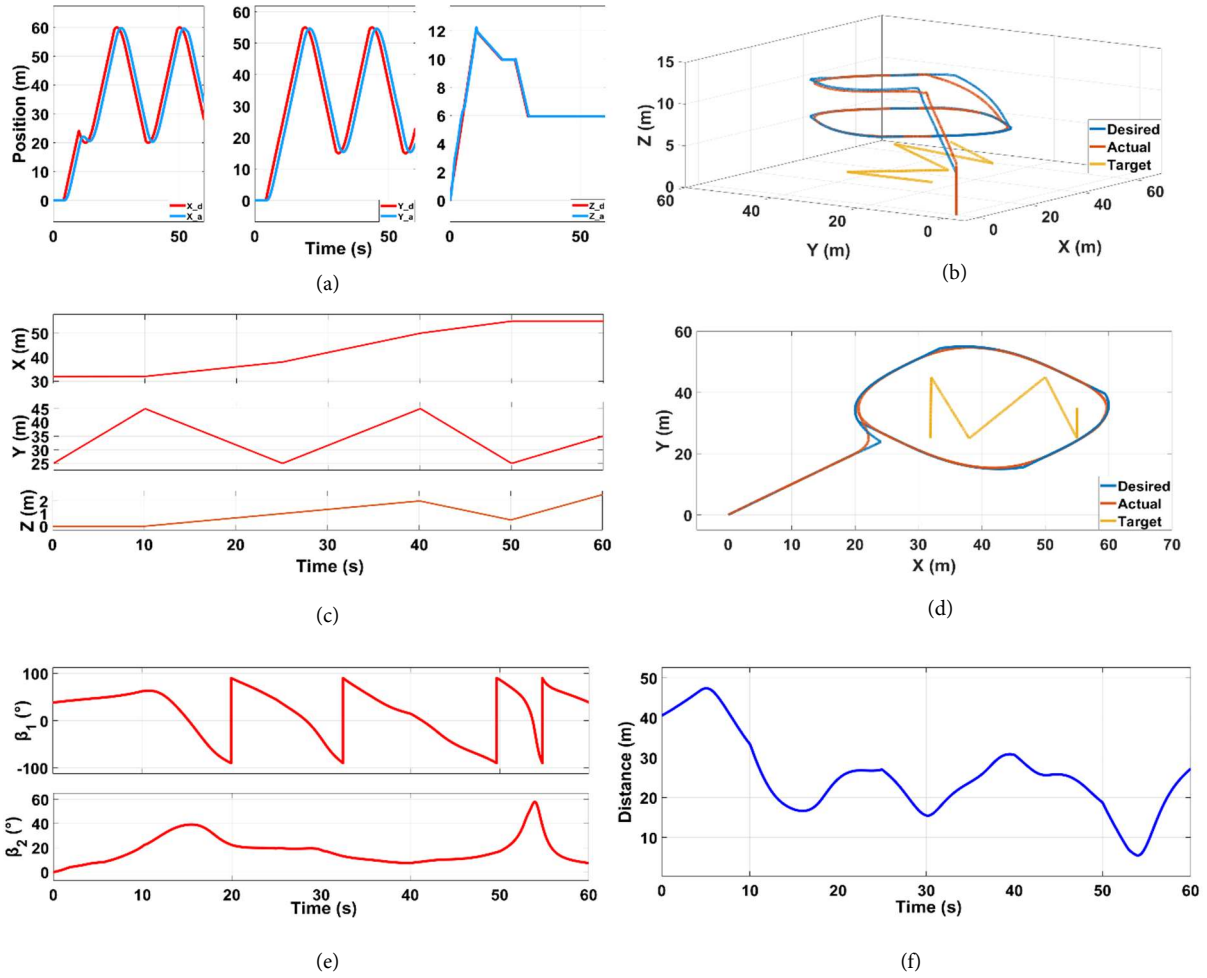

(a) (b) (c) (d) (e) (f)

Figure 8. Regarding the case of the target being mobile; Trajectory tracking graphic (a) and (b), position change of the target (c), position change of the UAV and the target in the horizontal plane (d), change in manipulator joint angles (e), change in distance between UAV and target (f)

Fig. 8 provides visual representations of this scenario:

The reference trajectory for each of the three axes separately (a). The reference trajectory and the trajectory followed by the UAV in three dimensions (b). The movement of the target along all three axes (c). Both the trajectory of the UAV and the path in which the target moves, specifically shown in the horizontal plane (d). Displays the values of the manipulator joint angles over time (e). It allows you to observe the specific angles assumed by the manipulator joints as the simulation progresses. These values are crucial for controlling and positioning the manipulator accurately. And it illustrates how the linear distance between the UAV and the target changes as a function of flight time (f). It shows the evolution of the distance over the course of the simulation, providing insights into the relative positioning of the UAV and the target. These visualizations help to illustrate the interaction between the UAV's trajectory and the target's movement in a dynamic environment.

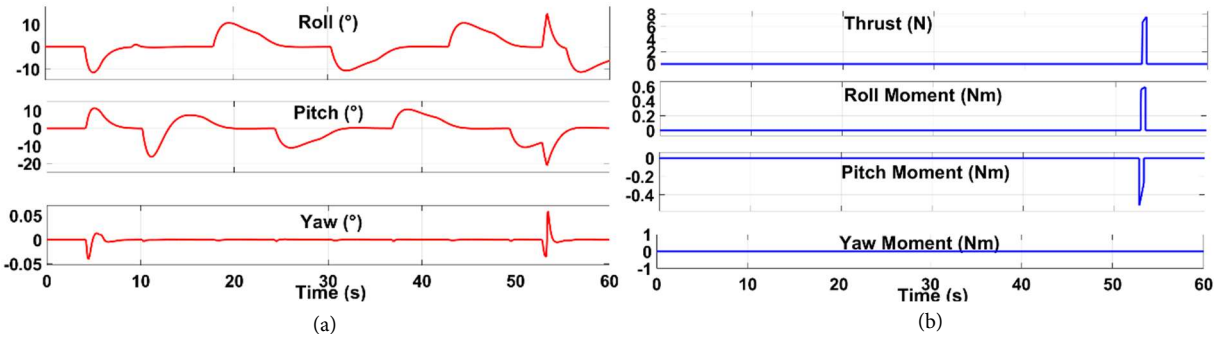

(a) (b)

Figure 9. Case of the moving target; Euler angles change graph (a), the effect of throw reaction force on roll, pitch and yaw moments, and thrust force (b)

The subplot, Fig. 9a, illustrates the changes in the roll, pitch, and yaw angles of the UAV throughout the flight. It shows how these angles evolve over time, providing insights into the UAV's orientation and rotational movements along each axis. The subplot, Fig. 9b, highlights the impact of the throw reaction force on the moments (roll, pitch, and yaw) and the thrust force of the UAV. It demonstrates how the throw reaction force affects the stability and control of the UAV by exerting moments and influencing the thrust force.

5. Experimental Setup

In the experiment, an open source flight control board, Pixhawk, is used to control the proposed UAV system with manipulator [1,46]. The board has fourteen outputs, eight of which are main outputs and six are auxiliary outputs. Necessary connections were made according to the layout order of the brushless motors on the relevant configuration by using four main outputs. And three auxiliary outputs are used for servo motors used in the manipulator. Although the control of the manipulator can be done using an external controller [47], it can also be controlled by writing the desired codes on the flight control card as a more practical method. As seen in Figure 10, Lua scripting is a coding which are run at a low priority on the system. This ensures that the core flight code will continue to execute even if a script is taking a long time to process. Lua Scripting provides a safe, “sandboxed” environment for new behaviors to be added to the autopilot without modifying the core flight code. And the scripts are run in parallel with the flight code [48]. The system established for experimental study is given in figure 11. Angular positions of the vehicle are taken from the gyro built into the flight controller. Similarly, linear position data of the vehicle is received from the GPS receiver connected to the flight controller. Both angular and translational position data received from the FCU include both internal and external disturbances. Therefore, to determine the joint angles of the manipulator, these data must be cleared of these distortions before being included in the mathematical process. Thus, a Kalman Filter is added to the Lua script where joint angles are calculated. Thus, the joint angles of the manipulator could be estimated more accurately. In addition, by manually entering the location data of the target into the system, the joint angles of the manipulator integrated into the UAV are calculated. Which is known by taking inverse kinematics calculation.

ISSN: 2149-9373

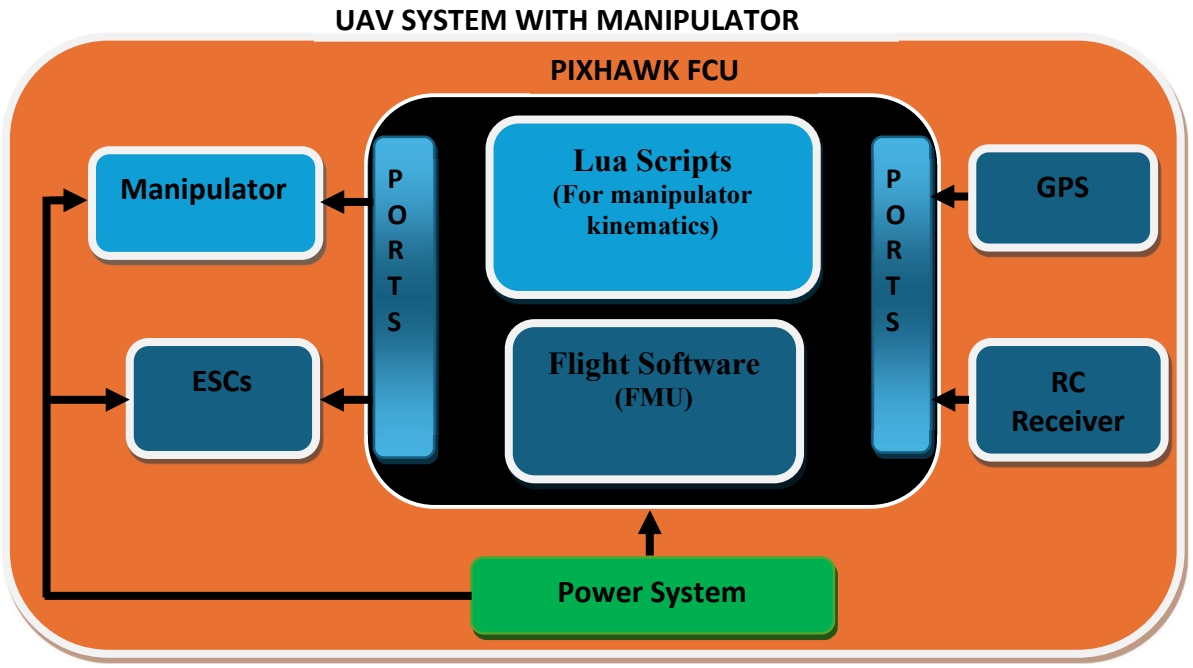

Figure 10. Schematic representation of whole systems for experiments

The calculated joint angles are converted to PWM values for the servo motors that provide the angular movement in the joints. The system is locked to the target by positioning the servo motors according to the PWM value.

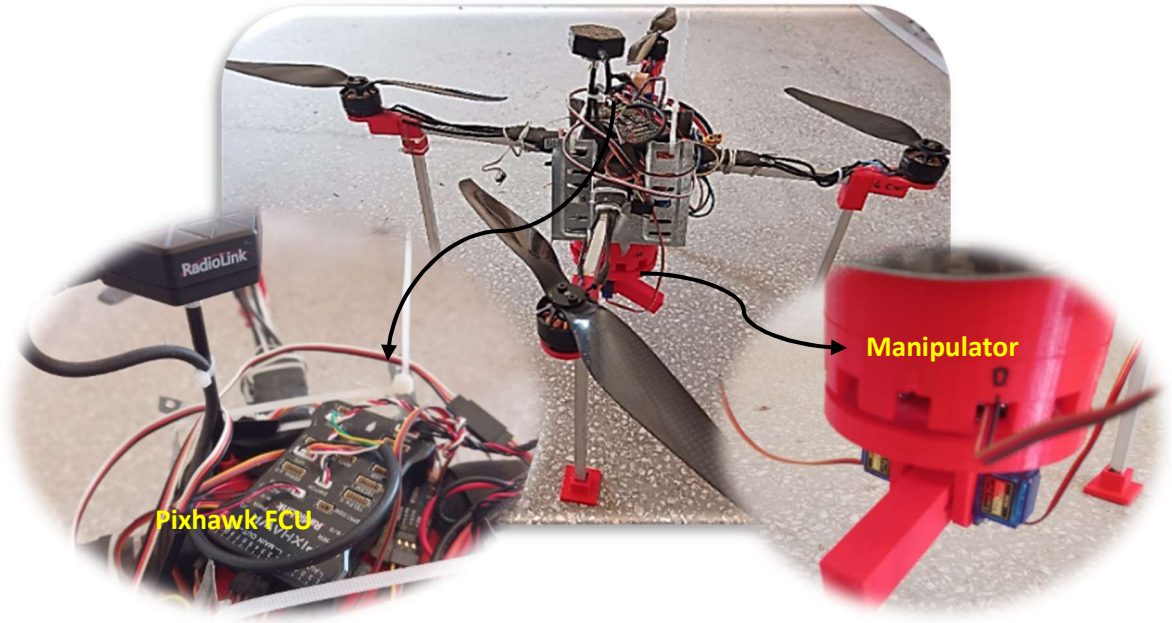

Figure 11. The UAV system with manipulator

The mentioned inverse kinematic calculation continues throughout the flight of the UAV. According to both attitude and altitude data received from the FCU, the control of two joints of the manipulator is carried out in an indoor environment. The location of the target was entered into the script manually. The working principal diagram of the entire system is given in **Hata! Başvuru kaynağı bulunamadı.**.

ISSN: 2149-9373

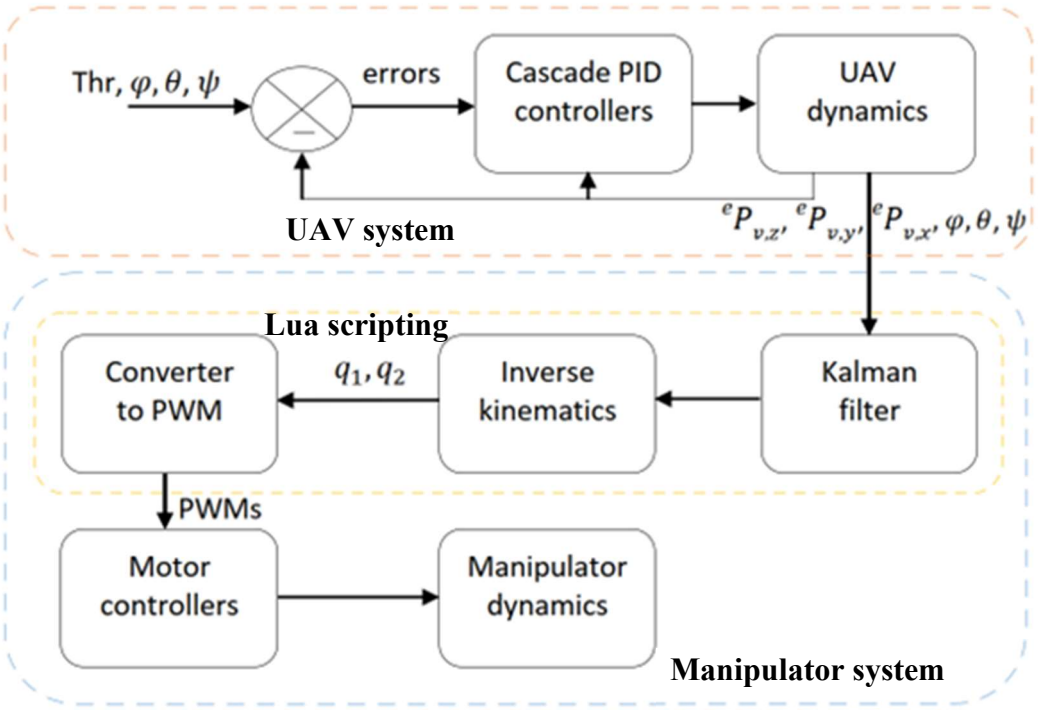

Figure 12. Controller structure of the system

In addition, the Lua scripting summary of the operation of the manipulator system is presented in Table 2. It should be noted that, for safety and regulatory considerations, full integration tests involving in-flight anesthesia needle launching are not conducted in this initial study. Instead, the focus is on validating the manipulator's control system under real UAV flight data and ensuring its ability to accurately target a fixed position.

Table 2. Working principle algorithm of the manipulator system

	Algorithm 1: Lua Scripting for control of manipulator
1	Determine Kalman parameter values
2	Assign Motor Outputs **(AUX1-AUX3)**
3	Determine initial positions of motors of the manipulator **(PWM1-PWM3)**
	function update ()
4	Get angular position data of the UAV **(roll, pitch, yaw)**
5	Get translational position data of the UAV **(Lat, Long, Alt)**
6	Get translational position data of the target **(Lat, Long, Alt)**
7	Filter data for the positions **(Target and UAV)**
8	Calculate manipulator angles ($\boldsymbol{q_1}$, $\boldsymbol{q_2}$)
9	Calculate required PWM values for motors **(PWM1-PWM3)**
	end

The proposed system is presented as a proof-of-concept, and future work will aim to perform comprehensive flight tests including live needle launching to evaluate the integrated system's performance under realistic dynamic conditions.

6. Discussion and Conclusion

In this study, a system has been proposed to address the complex and challenging task of capturing animals in real-life situations. This includes capturing wild animals in their natural habitats, rescuing stray animals, or managing farm animals. Animal capture often presents significant difficulties for officials and caretakers, requiring careful planning and execution. To tackle this problem, it has been proposed a system. The system consists of a quad-rotor UAV, equipped with a manipulator and an anesthetic needle throwing mechanism. This system aims to enhance the capture process by providing a remote anesthesia method facilitated by UAV technology. The UAV serves as the platform for the entire

system, allowing for autonomous flight and precise maneuvering. The manipulator integrated into the UAV provides the necessary dexterity and control to direct the anesthesia needle accurately. To validate the proposed system, firstly, it was conducted two simulations based on the mathematical model developed for the system. The simulations encompassed two scenarios: one with a stationary target and another with a target in motion. Through these simulations, it was evaluated the system's performance and its ability to effectively capture animals in different situations.

Secondly, in the experimental part, the manipulator angles could be controlled by processing the dynamic data of the UAV and the manipulator with the Lua Scripting code written on the flight control card. Here, the target is assumed to be in a fixed position. In outdoor tests, without flight, the manipulator was found to be quite sensitive to the target. The results demonstrated that the proposed system is indeed capable of addressing the challenges associated with animal capture. Overall, this study presents an innovative and practical solution for animal capture, utilizing the advancements in UAV technology and robotics. By combining the capabilities of a quad-rotor UAV, a manipulator, and an anesthetic needle throwing mechanism, the proposed system offers a promising approach to improve the efficiency and safety of animal capture operations. It opens up new possibilities for wildlife management, animal rescue efforts. On the other hand, it would be more appropriate for an operator to use this proposed system for the mentioned purpose. Although the UAV can be directed to the target autonomously and the manipulator is locked on the target, the operator can direct the UAV to the target with a camera integrated into the UAV. Thus, a more suitable result can be achieved by controlling the launch mechanism by the operator according to the location of the target. Autonomous target detection and tracking functionalities are not implemented in the current experimental setup. Instead, target coordinates are manually entered for preliminary validation of manipulator control based on UAV dynamics. The integration of a computer vision-based module for real-time detection and tracking is planned for future development, as it requires a separate algorithmic framework, and computational resources not addressed in this initial phase. In the current study, the camera serves as a supporting component for future operator-assisted control, which was briefly discussed in the conclusion section. Full autonomy, including onboard visual processing and real-time tracking, is considered outside the scope of this proof-of-concept work.

In addition to the controlled simulation and experimental results presented, it is important to acknowledge potential limitations that may arise in real-world applications. Environmental factors such as wind, target unpredictability, and system endurance, as well as legal and ethical considerations, may influence the effectiveness and safety of the proposed system. These challenges were not within the scope of this preliminary study. However, they are essential for the practical deployment of the system and will be addressed in future research. Table 3 summarizes the key real-world constraints identified and possible strategies to mitigate them.

Table 3. Potential Real-World Constraints and Suggested Mitigation Strategies

Constraint	Potential Impact	Suggested Mitigation or Future Work
Wind disturbances	Can alter UAV stability and needle trajectory, reducing hit accuracy	Incorporate wind compensation algorithms and onboard sensors; use heavier projectiles or stabilization fins
Battery life / Flight duration	Limits operational range and time; affects mission feasibility	Optimize energy efficiency, use higher capacity batteries, or swappable battery systems
Unpredictable animal movement	May cause misalignment or missed launches	Integrate real-time vision systems and adaptive targeting algorithms
GPS signal reliability (e.g., in forest)	Affects UAV localization and targeting accuracy	Combine GPS with inertial measurement units (IMU), visual odometry, or RTK-GPS for higher accuracy
Legal regulations	May restrict UAV flights or the use of tranquilizers in certain areas	Collaborate with local authorities, obtain necessary permits, and comply with UAV and veterinary laws
Ethical considerations	Concerns about animal welfare and operator safety	Conduct ethical reviews; apply guidelines for minimal intervention and humane capture
Payload weight limitations	Reduces available flight time and maneuverability	Use lightweight materials and miniaturized electronics

Conflict of Interest Statement

The authors declare that there is no conflict of interest

ISSN: 2149-9373

References

[1] Ş. Yıldırım, N. Çabuk, and V. Bakırcıoğlu, "Experimentally flight performances comparison of octocopter, decacopter and dodecacopter using universal UAV," *Measurement*, vol. 213, no. February, p. 112689, 2023. doi: 10.1016/j.measurement.2023.112689

[2] P. Shu, F. Li, J. Zhao, and M. Oya, "Robust Adaptive Control for A Novel Fully-Actuated Octocopter UAV with Wind Disturbance," *J. Intell. Robot. Syst. Theory Appl.*, vol. 103, no. 1, 2021. doi: 10.1007/s10846-021-01450-x

[3] N. Çabuk and Ş. Yıldırım, "Design, Modelling and Control of an Eight-Rotors UAV with Asymmetric Configuration for Use in Remote Sensing Systems," *J. Aviat.*, vol. 5, no. 2, pp. 72–81, Sep. 2021. doi: 10.30518/jav.943804

[4] V. Bakırcıoğlu, N. Çabuk, and Ş. Yıldırım, "Experimental comparison of the effect of the number of redundant rotors on the fault tolerance performance for the proposed multilayer UAV," Rob. Auton. Syst., vol. 149, p. 103977, Mar. 2022. doi: 10.1016/j.robot.2021.103977

[5] S. Li, Z. Lv, L. Feng, Y. Wu, and Y. Li, "Nonlinear Cascade Control for a New Coaxial Tilt-rotor UAV," *Int. J. Control. Autom. Syst.*, vol. 20, no. 9, pp. 2948–2958, 2022. doi: 10.1007/s12555-021-0105-1

[6] D. Sufiyan, L. S. T. Win, S. K. H. Win, Y. H. Pheh, G. S. Soh, and S. Foong, "An Efficient Multimodal Nature-Inspired Unmanned Aerial Vehicle Capable of Agile Maneuvers," *Adv. Intell. Syst.*, vol. 5, no. 1, p. 2200242, 2023. doi: 10.1002/aisy.202200242

[7] C. Vourtsis, V. C. Rochel, N. S. Müller, W. Stewart, and D. Floreano, "Wind Defiant Morphing Drones," *Adv. Intell. Syst.*, vol. 5, no. 3, pp. 1–8, 2023. doi: 10.1002/aisy.202200297

[8] C. Lee, S. Kim, and B. Chu, "A Survey: Flight Mechanism and Mechanical Structure of the UAV," *Int. J. Precis. Eng. Manuf.*, vol. 22, no. 4, pp. 719–743, 2021. doi: 10.1007/s12541-021-00489-y

[9] D. Ribeiro et al., "Non-contact structural displacement measurement using Unmanned Aerial Vehicles and video-based systems," *Mech. Syst. Signal Process.*, vol. 160, p. 107869, 2021. doi: 10.1016/j.ymssp.2021.107869

[10] A. Mitra, B. Bera and A. K. Das, "Design and Testbed Experiments of Public Blockchain-Based Security Framework for IoT-Enabled Drone-Assisted Wildlife Monitoring," *IEEE INFOCOM 2021 - IEEE Conference on Computer Communications Workshops (INFOCOM WKSHPS), Vancouver, BC, Canada, 2021*. pp. 1-6, doi: 10.1109/INFOCOMWKSHPS51825.2021.9484468

[11] S. Hirata, "Studying feral horse behavior from the sky," *Artif. Life Robot.*, vol. 27, no. 2, pp. 196–203, 2022. doi: 10.1007/s10015-022-00746-x

[12] Y. Cai et al., "Research on path generation and stability control method for UAV-based intelligent spray painting of ships," *J. F. Robot.*, vol. 39, no. 3, pp. 188–202, 2022. doi: 10.1002/rob.22044

[13] H. U. Unlu, D. Chaikalis, A. Tsoukalas, and A. Tzes, "UAV Indoor Exploration for Fire-Target Detection and Extinguishing," *J. Intell. Robot. Syst. Theory Appl.*, vol. 108, no. 3, 2023. doi: 10.1007/s10846-023-01835-0

[14] X. Liu, Z. R. Peng, L. Y. Zhang, and Q. Chen, "Real-time and Coordinated UAV Path Planning for Road Traffic Surveillance: A Penalty-based Boundary Intersection Approach," *Int. J. Control. Autom. Syst.*, vol. 20, no. 8, pp. 2655–2668, 2022. doi: 10.1007/s12555-020-0565-8

[15] H. Durgun, E. Yılmaz İnce, M. İnce, H. O. Çoban, and M. Eker, "Evaluation of Tree Diameter and Height Measurements in UAV Data by Integrating Remote Sensing and Machine Learning Methods," *Gazi J. Eng. Sci.*, vol. 9, no. 4, pp. 113–125, 2023. doi: 10.30855/gmbd.0705s12

[16] A. Altan and R. Hacıoğlu, "Model predictive control of three-axis gimbal system mounted on UAV for real-time target tracking under external disturbances," *Mech. Syst. Signal Process.*, vol. 138, p. 106548, Apr. 2020. doi: 10.1016/j.ymssp.2019.106548

[17] H. Yao, R. Qin, and X. Chen, "Unmanned aerial vehicle for remote sensing applications - A review," *Remote Sens.*, vol. 11, no. 12, pp. 1–22, 2019. doi: 10.3390/rs11121443

[18] A. Khan, S. Gupta, and S. K. Gupta, "Emerging UAV technology for disaster detection, mitigation, response, and preparedness," *J. F. Robot.*, vol. 39, no. 6, pp. 905–955, 2022. doi: 10.1002/rob.22075

[19] M. Karaduman, A. Çınar, and H. Eren, "UAV Traffic Patrolling via Road Detection and Tracking in Anonymous Aerial Video Frames," *J. Intell. Robot. Syst. Theory Appl.*, vol. 95, no. 2, pp. 675–690, 2019. doi: 10.1007/s10846-018-0954-x

[20] S. Hamaza et al., "Sensor Installation and Retrieval Operations Using an Unmanned Aerial Manipulator," *IEEE Robot. Autom. Lett.*, vol. 4, no. 3, pp. 2793–2800, 2019. doi: 10.1109/LRA.2019.2918448

[21] H. Bonyan Khamseh, F. Janabi-Sharifi, and A. Abdessameud, "Aerial manipulation—A literature survey," *Rob. Auton. Syst.*, vol. 107, pp. 221–235,

2018. doi: 10.1016/j.robot.2018.06.012

[22] E. L. de Angelis and F. Giulietti, "Stability and control issues of multirotor suspended load transportation: An analytical closed–form approach," *Aerosp. Sci. Technol.*, vol. 135, p. 108201, 2023. doi: 10.1016/j.ast.2023.108201

[23] E. Altuğ, M. E. Mumcuoğlu, I. Yüksel, and E. Altuğ, "Design of an Automatic Item Pick-up System for Unmanned Aerial Vehicles," *Celal Bayar Univ. J. Sci.*, vol. 16, no. 1, pp. 25–33, 2020. doi: 10.18466/cbayarfbe.529996

[24] B. V. Vidyadhara et al., "Design and integration of a drone based passive manipulator for capturing flying targets," *Robotica*, vol. 40, no. 7, pp. 2349–2364, 2022. doi: 10.1017/S0263574721001673

[25] M. F. Ballesteros-Escamilla, D. Cruz-Ortiz, I. Chairez, and A. Luviano-Juárez, "Adaptive output control of a mobile manipulator hanging from a quadcopter unmanned vehicle," *ISA Trans.*, vol. 94, pp. 200–217, 2019. doi: 10.1016/j.isatra.2019.04.002

[26] J. Liang, Y. Chen, N. Lai, and B. He, "Robust Observer-based Trajectory Tracking Control for Unmanned Aerial Manipulator," *Int. J. Control. Autom. Syst.*, vol. 21, no. 2, pp. 616–629, 2023. doi: 10.1007/s12555-021-0829-y

[27] W. Stewart, L. Guarino, Y. Piskarev, and D. Floreano, "Passive Perching with Energy Storage for Winged Aerial Robots," *Adv. Intell. Syst.*, vol. 5, no. 4, 2023. doi: 10.1002/aisy.202100150

[28] M. L. Guillen-Climent, P. J. Zarco-Tejada, J. A. J. Berni, P. R. J. North, and F. J. Villalobos, "Mapping radiation interception in row-structured orchards using 3D simulation and high-resolution airborne imagery acquired from a UAV," *Precis. Agric.*, vol. 13, no. 4, pp. 473–500, 2012. doi: 10.1007/s11119-012-9263-8

[29] S. Wang, J. Chen, and X. He, "An adaptive composite disturbance rejection for attitude control of the agricultural quadrotor UAV," *ISA Trans.*, vol. 129, pp pp. 564-579, Jan. 2022. doi: 10.1016/j.isatra.2022.01.012

[30] Z. Zheng et al., "An efficient online citrus counting system for large-scale unstructured orchards based on the unmanned aerial vehicle," *J. F. Robot.*, no. November 2022, pp. 552–573, 2022. doi: 10.1002/rob.22147

[31] X. Yang, X. Hu, H. Ye, W. Liu, and H. Shen, "Fraction-order MRAC Method Based Fault Tolerant Control for Plant Protection UAV With Actuator Failure and Uncertainty," *Int. J. Control. Autom. Syst.*, vol. 21, no. X, pp. 1–11, 2023. doi: 10.1007/s12555-021-1039-3

[32] Ş. Yıldırım and B. Ulu, "Deep Learning Based Apples Counting for Yield Forecast Using Proposed Flying Robotic System," *Sensors*, vol. 23, no. 13, p. 6171, Jul. 2023. doi: 10.3390/s23136171

[33] H. Ucgun, U. Yuzgec, and C. Bayilmis, "A review on applications of rotary-wing unmanned aerial vehicle charging stations," *Int. J. Adv. Robot. Syst.*, vol. 18, no. 3, 2021. doi: 10.1177/17298814211015863

[34] N. Yang et al., "Mapping potential human-elephant conflict hotspots with UAV monitoring data," *Glob. Ecol. Conserv.*, vol. 43, no. April, p. e02451, 2023. doi: 10.1016/j.gecco.2023.e02451

[35] X. Li and L. Xing, "Use of Unmanned Aerial Vehicles for Livestock Monitoring based on Streaming K-Means Clustering," *IFAC-PapersOnLine*, vol. 52, no. 30, pp. 324–329, 2019. doi: 10.1016/j.ifacol.2019.12.560

[36] N. Rey, M. Volpi, S. Joost, and D. Tuia, "Detecting animals in African Savanna with UAVs and the crowds," *Remote Sens. Environ.*, vol. 200, no. March, pp. 341–351, 2017. doi: 10.1016/j.rse.2017.08.026

[37] J. C. Hodgson, D. Holman, A. Terauds, L. P. Koh, and S. D. Goldsworthy, "Rapid condition monitoring of an endangered marine vertebrate using precise, non-invasive morphometrics," *Biol. Conserv.*, vol. 242, no. January, p. 108402, 2020. doi: 10.1016/j.biocon.2019.108402

[38] G. N. C. Inoue et al., "Combined spinal and general anesthesia attenuate tumor promoting effects of surgery. An experimental animal study," *Ann. Med. Surg.*, vol. 75, no. February, 2022. doi: 10.1016/j.amsu.2022.103398

[39] T. Bleeser, T. R. Hubble, M. Van de Velde, J. Deprest, S. Rex, and S. Devroe, "Introduction and history of anaesthesia-induced neurotoxicity and overview of animal models," *Best Pract. Res. Clin. Anaesthesiol.*, vol. 37, no.1, pp. 3-15, 2023. doi: 10.1016/j.bpa.2022.11.003

[40] A. K. O. Alstrup, M. R. Dollerup, M. I. T. Simonsen, and M. H. Vendelbo, "Preclinical Imaging Studies: Protocols, Preparation, Anesthesia, and Animal Care," *Semin. Nucl. Med.*, 2023. doi: 10.1053/j.semnuclmed.2023.02.003

[41] N. Pharmaceuticals, "WILDLIFE DARTING EQUIPMENT," NexGen Pharmaceuticals, 2021. https://nexgenvetrx.com/blog/nondomesticsexotics/immobilizationsedation/wildlife-darting-equipment/ [Accessed Jun. 04, 2023].

[42] J. Ortiz, M. Ando, and T. Miyazaki, "Numerical Simulation of Wind Drift of Arrows on the Olympic Venue for Tokyo 2020," *Athens J. Sport.*, vol.

7, no. 1, pp. 1–20, 2020. doi: 10.30958/ajspo.7-1-1

[43] J. O. Hampton et al., "Animal welfare testing for shooting and darting free-ranging wildlife: a review and recommendations," *Wildl. Res.*, vol. 48, no. 7, p. 577, 2021. doi: 10.1071/WR20107

[44] N. Çabuk, "Design and walking analysis of proposed four-legged glass cleaning robot," *Turkish J. Eng.*, vol. 7, no. 2, pp. 82–91, 2023. doi: 10.31127/tuje.1011320

[45] M. A. Şen, V. Bakırcıoğlu, and M. Kalyoncu, "Inverse Kinematic Analysis of A Quadruped Robot," *Int. J. Sci. Technol. Res.*, vol. 6, no. 9, pp. 285–289, 2017, [Online]. Available: http://ethesis.nitrkl.ac.in/6980/1/2015_Panchanand_Phd_511ID101.pdf

[46] E. Ebeid, M. Skriver, K. H. Terkildsen, K. Jensen, and U. P. Schultz, "A survey of Open-Source UAV flight controllers and flight simulators," *Microprocess. Microsyst.*, vol. 61, pp. 11–20, Sep. 2018. doi: 10.1016/j.micpro.2018.05.002

[47] N. Çabuk, "Design and Experimental Validation of an Adaptive Landing Gear for Safe Landing on Uneven Grounds of VTOL UAVs in the Context of Lightweight and Fast Adaptations," *Arab. J. Sci. Eng.*, vol. 48, no. 9, pp. 12331–12344, Sep. 2023. doi: 10.1007/s13369-023-07731-x

[48] ArduPilot Dev Team, "Advanced Configuration (Lua Scripts)," 2023. Available: https://ardupilot.org/copter/docs/common-lua-scripts.html. [Accessed: Oct. 12, 2024].